Received: 2 April 2024 | Revised: 22 May 2024 | Accepted: 5 June 2024

DOI: 10.1002/agt2.627

Aggregate WILEY

RESEARCH ARTICLE

Sulfato-β-cyclodextrin induced multivalent supramolecular directional aggregation of cyanovinylene derivatives for achieving reversible near-infrared fluorescence

Zhixue Liu[1] | **Haiqi Chen**[1] | **Mengdi Tian**[2] | **Xinyao Sun**[1] | **Yong-Xue Li**[2] | **Jie Wu**[2] | **Ruotong Wang**[1] | **Bin Li**[1] | **Chunju Li**[1] | **Yu Liu**[2]

[1]Tianjin Key Laboratory of Structure and Performance for Functional Molecules, College of Chemistry, Tianjin Normal University, Tianjin, P. R. China

[2]College of Chemistry, State Key Laboratory of Elemento-Organic Chemistry, Nankai University, Tianjin, P. R. China

Correspondence
Chunju Li, Tianjin Key Laboratory of Structure and Performance for Functional Molecules, College of Chemistry, Tianjin Normal University, Tianjin 300387, P. R. China.
Email: cjli@shu.edu.cn

Yu Liu, College of Chemistry, State Key Laboratory of Elemento-Organic Chemistry, Nankai University, Tianjin 300071, P. R. China.
Email: yuliu@nankai.edu.cn

Funding information
National Natural Science Foundation of China, Grant/Award Numbers: 21971192, 21807038; Tianjin Municipal Education Commission, Grant/Award Number: 2021KJ188; China Postdoctoral Science Foundation, Grant/Award Number: 2021T140343

Abstract

Molecular aggregation or supramolecular aggregation-induced emission is one of the research hotspots in chemistry, biology, and materials. Herein, we report negatively charged sulfato-β-cyclodextrin (SCD) induced cyanovinylene derivatives (DPy-6C) directional aggregation to form regular nanorods (DPy-6C@SCD) through supramolecular multivalent interactions, not only achieves ultraviolet-visible absorption redshifted from 453 to 521 nm but also displays near-infrared (NIR) aggregation-induced emission with a large spectral redshift of 135 nm. The DPy-6C monomer presents random nanosheets with weak fluorescence but obtains regular aggregates after assembly with SCD through electrostatic interactions. In the presence of H^+, the DPy-6C@SCD can further aggregate into elliptical nanosheets without fluorescence changes due to the protonation of secondary amines. In contrast, the morphology of DPy-6C@SCD becomes flexible and sticks together upon the addition of OH^- with an emission blue shift of 72 nm and a 90-fold intensity increase because of disrupting the stacking mode of aggregates, thereby achieving acid-base regulated reversible fluorescence behaviors that cannot be realized by DPy-6C monomer. The DPy-6C@SCD can efficiently select the detection of volatile organic amines both in liquid and gas phases within 5 s at the nanomolar level. Taking advantage of RGB analysis and calculation formula application, the DPy-6C@SCD has been successfully used to monitor various organic amines on a smartphone, accompanied by naked-eye visible photoluminescence. Therefore, the present research provides an efficient directional aggregation method through supramolecular multivalent interactions, which not only realizes topological morphology transformation but also achieves reversible NIR luminescent molecular switch and high sensitivity organic amines fluorescent sensing devices.

KEYWORDS
directional aggregation, multicharged cyclodextrins, near-infrared fluorescence emission, smartphone detection, supramolecular aggregates

1 | INTRODUCTION

Macrocycle-induced aggregation based on supramolecular multivalent interactions possessing morphology-controlled, luminescence improvement and multistimulus-responsive characters, which have broad application prospects in the fields of drug delivery,[1] topological morphology control,[2] chiral regulation and inversion,[3] luminescent materials,[4] information encryption and prevention,[5] and energy transfer.[6] The commonly used macrocycles such as cyclodextrins,[7] cucurbit[*n*]urils,[8] pillar[*n*]arenes,[9] cyclophanes and cages,[10] and other macrocyclic derivatives[11] can selectively bind guest molecules,[12] not only increased the water-solubility of guests, but also significantly improved their luminescent performance with multifunctional properties.[13] At present, macrocycle-induced emission behaviors can be divided into emission enhancement and quenching, emission blue shift and redshift. All these

phenomena were dependent on the macrocycle-based noncovalent interactions,[14] which changed the aggregation pattern of the guest molecules, resulting in various optical behaviors. Among them, macrocycle-induced emission redshift can generate new fluorescence bands in long wavelengths through intermolecular interactions in the aggregation state,[15] making an important contribution to constructing multifunctional near-infrared (NIR) supramolecular luminescent materials.

To some extent, some organic luminescent dyes cannot efficiently obtain emission redshift behaviors due to the weak self-aggregation capability under low concentration conditions in aqueous solution. Fortunately, macrocycle-induced aggregation can accelerate to achieve this process, because macrocycles can encapsulate guest molecules at low concentrations, resulting in the dimer or aggregate luminescence.[15b,16] For example, Park and coworkers reported that cucurbit[8]uril can encapsulate cyanostilbene derivatives to form supramolecular block copolymers with fluorescence emission redshift due to the strong intermolecular interactions of guests.[17] Huang and coworkers selected anionic pillar[5]arenes to assemble with cationic cyanostilbene derivatives through host-guest interactions to form enhanced NIR emission nanoparticles for living cell imaging.[18] It can be seen that a significant emission spectrum redshift of guests can be achieved by using host-guest encapsulation. However, the encapsulation of guest molecules usually requires macrocyclic hosts with size-matched cavities. In contrast, the electrostatic assembly induced by the multicharged macrocycles was another effective strategy to achieve aggregation-induced emission redshift,[19] which may ignore the cavity size of macrocycles. This is because multicharged macrocycles can significantly reduce the critical aggregation concentration of the guest molecules, resulting in a close-packing pattern at low concentrations.[20] And a small number of multicharged macrocycles can induce a large number of guest molecules to aggregate, which is conducive to realizing aggregate luminescence.[21]

In order to maximize molecular aggregation luminescence, non-aromatic macrocycles are a good choice because they can effectively avoid the fluorescence quenching or energy transfer of guests by aromatic groups on the macrocyclic skeleton.[22] In the reported non-aromatic macrocycles, α-, β-, and γ-cyclodextrins constructed from D-glucose units with different hydrophobic cavities are good macrocyclic candidates.[23] They can selectively confine guest molecules to induce or increase the fluorescence and phosphorescence behaviors,[24] as well as generate large Stokes shift and NIR emission.[25] Especially, multicharged cyclodextrins such as sulfato-β-cyclodextrin, sulfobutylether-β-cyclodextrin, and sugammadex sodium, possessing both hydrophobic cavities and multiple charges, can encapsulate or aggregate guests to form functional assembly through multivalent interactions.[26] Our group reported that copolymers of bromonaphthylpyridinium and diarylethene derivatives can coassemble with sulfobutylether-β-cyclodextrin, exhibiting reversible phosphorescence emission.[27] It can be found that multicharged cyclodextrin derivatives can quickly induce guest orderly aggregation through electrostatic interactions, which obviously changed the morphology and optical property of the guest molecules. Although the emission spectrum has not yet reached the NIR region, the electrostatic assembly strategy is still an effective method, because the NIR luminescence behaviors of the aggregates can be controlled by the structure of the guests. Therefore, multicharged cyclodextrin derivatives can serve as excellent macrocyclic hosts to construct NIR luminescent materials with large emission spectrum redshift through supramolecular multivalent interactions. By means of dynamic and reversible noncovalent interactions from multicharged macrocycles, the formed aggregates can also obtain multiple stimulus responsiveness,[28] which can be used to construct molecular switches and supramolecular intelligent devices.

Herein, we constructed multicharged cyclodextrin-induced aggregates based on cyanovinylene derivatives (DPy-6C) and sulfato-β-cyclodextrin (SCD) through electrostatic interactions, π-π interactions, and hydrophobic interactions (Scheme 1). Due to the formation of regular aggregates, the ultraviolet-visible (UV-vis) absorption of DPy-6C redshifted from 453 to 521 nm with the maximum fluorescence emission redshifted from 530 to 665 nm upon the addition of SCD, accompanied by the morphology of DPy-6C changed from random nanosheets to regular nanorods. The DPy-6C@SCD exhibits obvious pH-response capability, especially to OH^-, in which the fluorescence emission blue-shifted about 72 nm and the intensity was enhanced by about 90 times, accompanied by the morphology becoming flexible and stuck together. The DPy-6C@SCD can serve as a good luminescent platform for rapidly sensing volatile organic amines within 5 s. Taking advantage of the sensing process with RGB analysis and calculation formula application, the content of organic amines can be rapidly and semi-quantitatively detected on a smartphone.

2 | RESULTS AND DISCUSSION

First, the UV-vis absorption and fluorescence spectra of DPy-6C were investigated under different solvent compositions. The maximum UV-vis absorption peak of DPy-6C showed an obvious redshift of 31 nm when the water content was changed from 0% to 99%, accompanied by the fluorescence emission spectrum redshift of 25 nm (Figure 1A), indicating that DPy-6C can uniformly disperse in tetrahydrofuran and aggregated in aqueous solution. Because cyanovinylene dyes can aggregate to form a dimer and exhibit a more orderly aggregation pattern with redshift luminous behavior in a solid or crystalline state.[29] In order to improve the aggregation extent of DPy-6C in aqueous solution, negatively charged SCD (12 mol SO_3Na per 1 mol SCD) was employed to assembly with DPy-6C through electrostatic interactions, aiming to achieve efficient dimer luminescence of DPy-6C in aqueous solution. Obviously, as shown in Figure 1B, the maximum UV-vis absorption peak of DPy-6C at 453 nm gradually decreased upon the addition of SCD, accompanied by the simultaneous appearance of a new absorption peak at 521 nm and the color changed from yellow to orange (Figure 1B inset). Meanwhile, the maximum fluorescence emission at 530 nm was also redshifted to 665 nm, and the fluorescence changed from yellow to deep red (Figure 1C, inset). The above results indicated that SCD can obviously induce DPy-6C aggregate into a tightly packed mode through electrostatic interactions and π-π interactions,

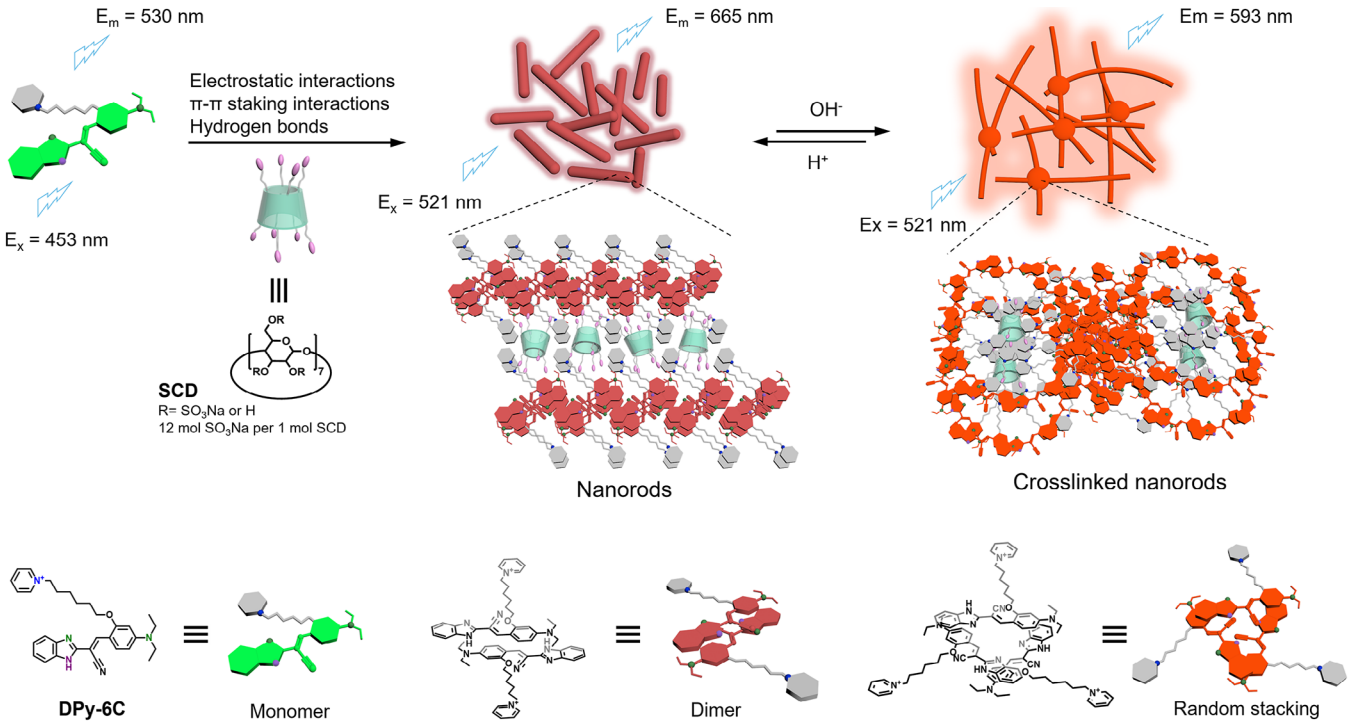

SCHEME 1 Schematic illustration of the possible assembly mechanism between DPy-6C and sulfato-β-cyclodextrin (SCD), as well as the reversible response of the DPy-6C@SCD to acid and base.

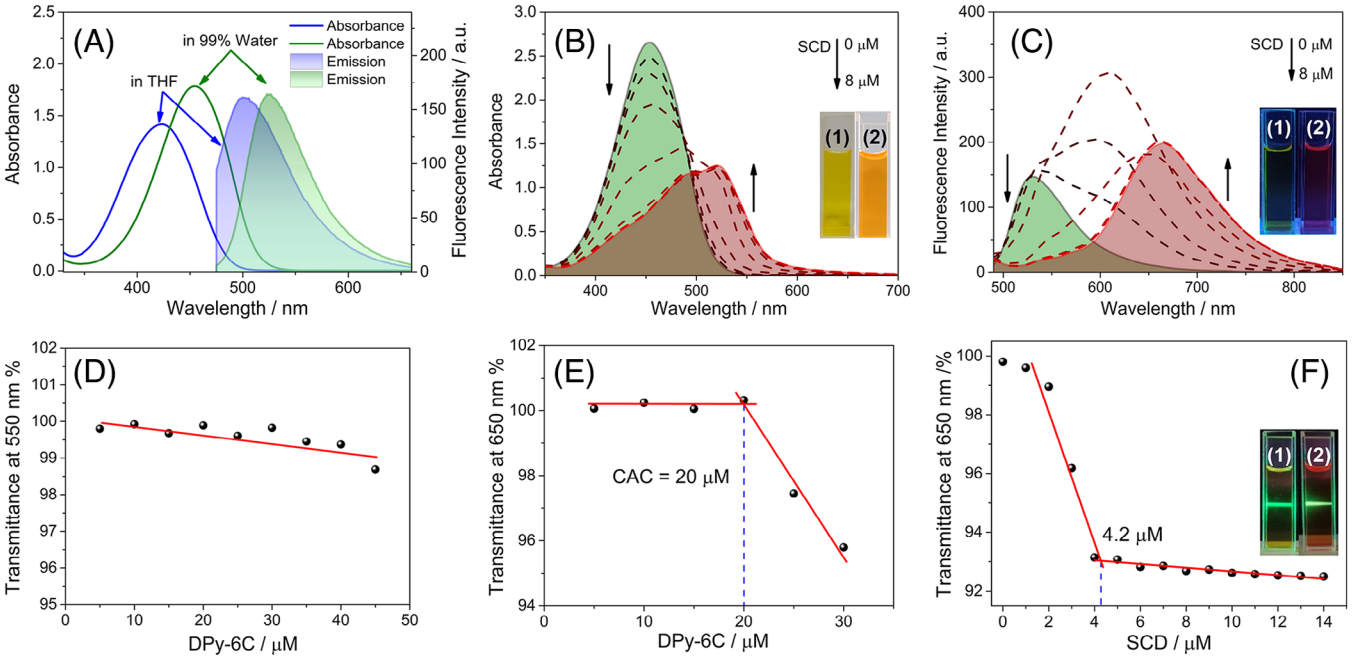

FIGURE 1 (A) Ultraviolet-visible (UV-vis) absorption and fluorescence spectra of DPy-6C (40 μM) under the condition of H_2O and tetrahydrofuran (THF) (Ex = 453 nm; slits: 10/10 nm). (B) UV-vis absorption and (C) fluorescence spectra of DPy-6C (40 μM) upon addition of sulfato-β-cyclodextrin (SCD) (0–8 μM) in aqueous solution (Ex = 453 nm; slits: 10/10 nm). Inset (B): Photographs of (1) DPy-6C and (2) DPy-6C@SCD; Inset (C): Photographs of (1) DPy-6C and (2) DPy-6C@SCD under 365 nm irradiation. (D, E) Optical transmittance changes of DPy-6C in the absence of SCD and the presence of SCD (2 μM), respectively. (F) Optical transmittance changes of DPy-6C (40 μM) with the different concentrations of SCD. Inset (F): Tyndall effects exhibited by (1) DPy-6C and (2) DPy-6C@SCD.

which efficiently restrict the rotation of DPy-6C, thereby resulting in significant changes in color and fluorescence. During this process, it is easy to observe that an intermediate state of the aggregation is experienced in fluorescence emission at 609 nm. This is because DPy-6C has the property of aggregation-induced emission, which may cause fluorescence emission redshift through random aggregation by a small amount of SCD. Therefore, the intermediate state of DPy-6C@SCD can obtain fluorescence enhancement with a redshift of 79 nm, but the equilibrium state of DPy-6C@SCD with sufficient SCD can form a more orderly aggregate with a redshift of about 135 nm.

On the other hand, the aggregation process of DPy-6C and SCD was further evaluated by measuring the optical transmittance. In the absence of SCD, the optical transmittance of DPy-6C decreased slightly with the increase in its concentration (Figure 1D and Figure S1A). In contrast, the optical transmittance of DPy-6C decreased rapidly after assembly with SCD, and the plot of optical transmittance versus DPy-6C concentration indicated that the critical aggregation concentration (CAC) was about 20 μM (Figure 1E and Figure S1B). As the SCD content increased, the optical transmittance decreased to 93% and remained stable (Figure 1F and Figure S1C). Based on the concentration ratio of SCD to DPy-6C, the optimal molar ratio of SCD:DPy-6C is calculated to be about 1:9.5. Compared with DPy-6C, DPy-6C@SCD solution showed a significant Tyndall effect (Figure 1F inset), indicating the formation of abundant supramolecular aggregates. Hence, it can be inferred that the SCD can effectively induce the fast aggregation of DPy-6C and obtain a stable aggregate, not only decreasing the CAC but also realizing the UV-vis absorption redshifted and NIR emission, accompanied by the fluorescence change from yellow to deep red. In addition. The job plot was performed to confirm the stoichiometry of DPy-6C and SCD in the assemblies. As shown in Figure S2, the binding stoichiometry between SCD and DPy-6C was validated as 1:9 from the Job plot. This is because the average degree of sulfonic acid in SCD is about 12, which means that each SCD has about 12 negative charges, and each DPy-6C contains only 1 positive charge. The theoretically binding stoichiometry of SCD and DPy-6C is about 1:12 due to the electrostatic interactions. The experimental test result displayed that the actual test value was close to the theoretical value, as well as consistent with the optimal molar ratio calculated from the optical transmittance. Therefore, the driving force between the DPy-6C and SCD was mainly from the electrostatic interactions.

Since DPy-6C is a cyanovinylene derivative, it is possible that the above aggregation changes are caused by the close accumulation of excimer. Therefore, the central luminescent skeleton without alkyl chain pyridine salts was synthesized, named DOMe, and its crystal structure was obtained (Figure S3). The crystal structure displayed that DOMe is arranged into offset columnar stacks of antiparallel dimers with close intermolecular stacking distances (3.461 Å) and obvious π-π interactions (3.950 Å). We deduced that the DPy-6C can assemble with SCD to form a similar excimer emission, and the possible assembly mode was J-aggregate. On the other hand, the chemical shift of the aromatic part of DPy-6C moves towards the lower field after adding a small amount of SCD, and then the solid is completely precipitated after adding a sufficient amount of SCD due to the aggregation (Figure S4). Hence, it can be inferred that π-π interactions existed when DPy-6C assembly with SCD.

In order to better characterize the morphological changes during the assembly process, the DPy-6C, DPy-6C@SCD intermediated state and DPy-6C@SCD equilibrium state were measured by transmission electron microscopy (TEM) and scanning electron microscopy (SEM). The TEM and SEM photographs displayed that the DPy-6C was irregular nanofragments (Figure 2A,C). After assembly with a small amount of SCD, the DPy-6C@SCD intermediated state gave irregular nanoparticles that stuck together, indicating the efficient assembly between DPy-6C and SCD (Figure S5). In contrast, the DPy-6C@SCD with enough SCD showed apparently regular nanorods with lengths of about 400 nm and a diameter of about 30 nm (Figure 2B,D). According to the morphologic transformation, it can be confirmed that the SCD obviously changed the aggregation mode of DPy-6C through electrostatic interactions and π-π interactions. Meanwhile, the fluorescence quantum yields of DPy-6C, DPy-6C@SCD intermediated state, and DPy-6C@SCD equilibrium state were measured to be 0.33%, 0.67%, and 0.63%, respectively (Figure S6). The lifetime of DPy-6C, DPy-6C@SCD intermediated state, and DPy-6C@SCD equilibrium state were measured to be 0.07, 0.50, and 1.68 ns, respectively (Figure S7). The changes in lifetime indicate that SCD can successfully assemble with DPy-6C to form supramolecular aggregates.

Structurally, the DPy-6C has an alkyl chain containing six carbons, hence, in order to investigate the role of the alkyl chain in the assembly process, the guest molecules containing a three-carbon alkyl chain (DPy-3C), four-carbon alkyl chain (DPy-4C), eight-carbon alkyl chain (DPy-8C) were synthesized and their aggregate behaviors were also evaluated. As shown in Figures S8A and S9, SCD can also induce DPy-3C, DPy-4C, and DPy-8C aggregate to generate a new absorption peak at 521 nm. However, the absorption coefficients of DPy-3C@SCD ($\varepsilon = 1.15\times10^4$ M^{-1} cm^{-1}), DPy-4C@SCD ($\varepsilon = 1.23\times10^4$ M^{-1} cm^{-1}) and DPy-8C@SCD ($\varepsilon = 0.91\times10^4$ M^{-1} cm^{-1}) were lower than that of DPy-6C@SCD ($\varepsilon = 3.15\times10^4$ M^{-1} cm^{-1}), indicating that the assembly capacity of DPy-3C, DPy-4C, DPy-8C and SCD was weaker than that of DPy-6C. The results indicated that eight carbon alkyl chain derivatives DPy-8C did not obtain the best aggregation, which implied that an excessively long carbon alkyl chain may lead to self-aggregation enhancement. In addition, the change of optical transmittance is not obvious (Figure S8B), and the fluorescence emission of DPy-3C@SCD only redshifted to 631 nm, which the redshift was 35 nm smaller than that of DPy-6C@SCD (Figure S8C,D). Therefore, the appropriate alkyl chain length played an important role in generating large emission redshift in supramolecular aggregates.

Circular dichroism spectra were further evaluated to explore the assembly mechanism. As shown in Figure S10A, DPy-6C has no cotton effect in aqueous solution. However, upon the addition of SCD in the DPy-6C solution, the cotton effect of DPy-6C@SCD was very obvious. It means that the SCD can induce the aggregation of DPy-6C to form a stable assembly with an obvious circular dichroism signal. In contrast, the circular dichroism spectra of DPy-3C and DPy-3C@SCD all displayed no cotton effect (Figure S10B), confirming that even though the SCD can induce aggregation of DPy-3C, the aggregation mode was different from DPy-6C@SCD. TEM photographs also displayed that the morphology of DPy-3C was nanorods, and then changed to twisted nanosheets after assembly with SCD (Figure S11), which was significantly different from DPy-6C@SCD morphology. Since cyclodextrins have chiral hydrophobic cavities, they can encapsulate molecules to achieve a chiral signal. Therefore, the binding behaviors of DPy-6C with parent β-CD and γ-CD were studied to confirm the host-guest encapsulation. As shown in Figure S12, the DPy-6C displayed no obvious change after the addition of β-CD or

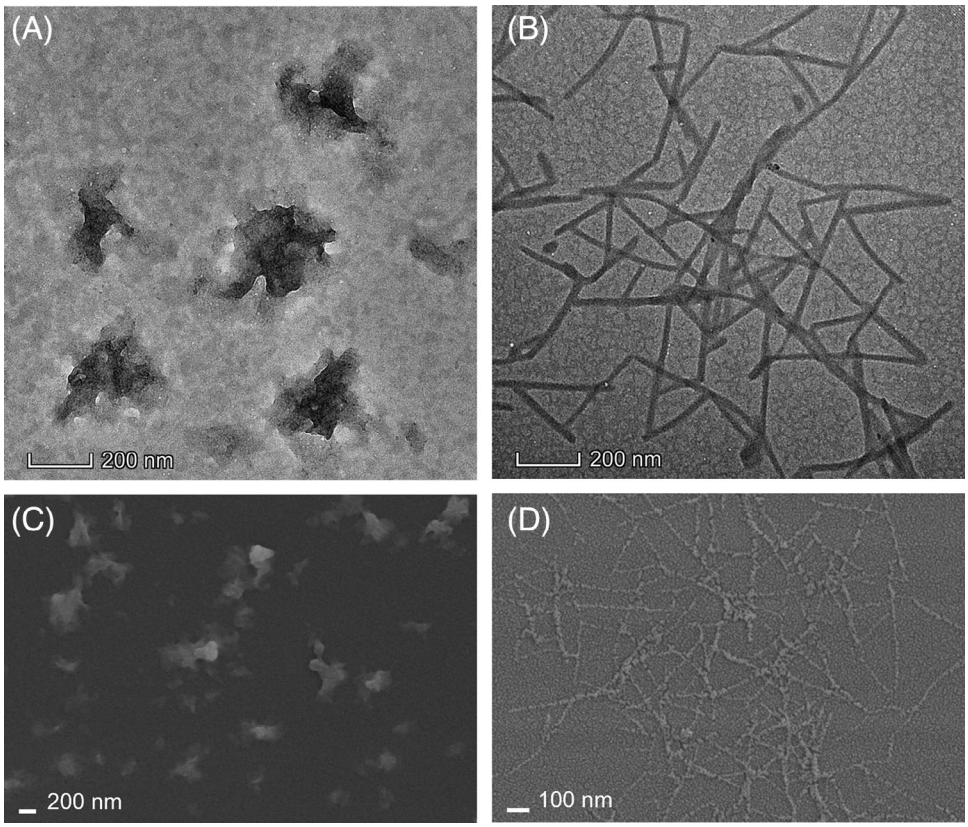

FIGURE 2 Transmission electron microscopy (TEM) and scanning electron microscopy (SEM) image of (A, C) DPy-6C and (B, D) DPy-6C@SCD.

γ-CD, meaning that there is no host-guest encapsulation. On the other hand, once the guests were wrapped into the SCD cavity, both DPy-3C and DPy-6C displayed similar cotton effects, but the results were the opposite, thereby indicating that the guests were assembled around the port of SCD, rather than in the SCD cavity.

In the structure of DPy-6C, the tertiary amines can be protonated in the presence of H^+, which will affect the luminescence behaviors. Therefore, the effect of H^+ and OH^- on the UV-vis absorption and fluorescence spectra of DPy-6C and DPy-6C@SCD were investigated, respectively. As shown in Figure 3A, in the absence of SCD, the UV-vis absorbance peak of DPy-6C decreased a little after the addition of OH^- and redshifted 25 nm after adding H^+. Meanwhile, the fluorescence intensity of DPy-6C was only enhanced by 1.5 times upon the addition of OH^- and redshifted 14 nm in the presence of H^+. In contrast, the UV-vis absorbance of DPy-6C@SCD redshifted about 7 nm after adding H^+ with the color changed from orange to orange-red in the presence of SCD (Figure 3B). The reason may come from the further aggregation between the protonated N-atom of DPy-6C (double charge or triple charge) and SCD. When the OH^- was added to the DPy-6C@SCD solution, the absorbance at 550 nm decreased without any color change (Figure 3C). The reason may be that the presence of bases affects the chemical shift of proton on benzimidazole (Figure S13), thereby disturbing the intermolecular staking of DPy-6C in the aggregation state. Interestingly, the fluorescence of the DPy-6C@SCD showed a big difference for H^+ and OH^-. The DPy-6C@SCD displayed negligible fluorescence change upon the addition of H^+ (Figure 3D). However, the maximum fluorescence emission of DPy-6C@SCD at 665 nm blue shifted to 593 nm after adding 149.4 μM OH^- (Figure 3E), and the fluorescence changed from red to orange with a significant enhancement of about 90 times. During the titration of H^+ or OH^-, the UV-vis changes of DPy-6C@SCD did not change to DPy-6C monomer, indicating that the DPy-6C@SCD did not undergo disassembly in this process. According to the response results of DPy-6C and DPy-6C@SCD, it can be found that the DPy-6C is not sensitive to OH^- and H^+, while the assembly of DPy-6C@SCD gave noticeable changes to OH^-. Subsequently, the reversible fluorescence intensity changes of DPy-6C@SCD toward OH^- and H^+ at 593 nm were evaluated (Figure 3F and Figure S14). After alternating OH^- and H^+ cycles five times, DPy-6C@SCD showed good reversibility without any attenuation and fatigue. Even though DPy-3C@SCD displayed responsibility to OH^- and H^+, the change was smaller than that of DPy-6C@SCD and the fluorescence intensity was also weak (Figure S15). The above results indicate that the assembly of DPy-6C@SCD possesses better responsibility to OH^- than that of DPy-6C and DPy-3C@SCD, which could serve as a good indicator to identify OH^-.

The morphological changes of DPy-6C@SCD to H^+ and OH^- were further measured by TEM and SEM. When H^+ was added to DPy-6C@SCD solution, the nanorods were changed to elliptical nanosheets with a long axis of 500 nm and a short axis of 250 nm (Figure 4A,C). In contrast, the nanorods of DPy-6C@SCD became flexible and stuck together with the addition of OH^- (Figure 4B,D). The morphological changes demonstrated that the assembly of DPy-6C@SCD did not disassemble into DPy-6C in the presence of H^+ or OH^-, but in another aggregation manner. In order to investigate the assembly mechanism of DPy-6C@SCD to H^+. The reference molecule DBr-6C without positive charge was selected for assembly with SCD. As

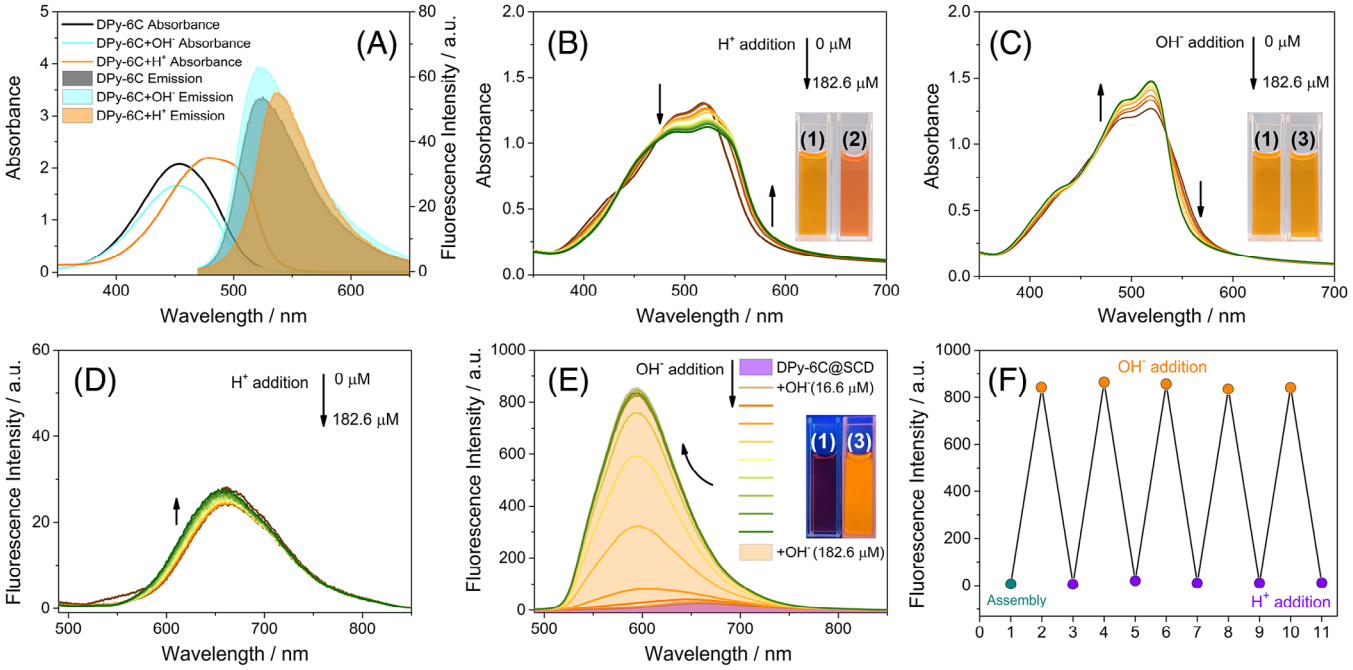

FIGURE 3 (A) Ultraviolet-visible (UV-vis) absorption and fluorescence spectra of DPy-6C (40 μM) under the condition of HCl and NaOH (Ex = 453 nm; slits: 10/10 nm). (B, C) UV-vis absorption and (D, E) fluorescence spectra of DPy-6C@SCD (40 μM) upon addition of HCl and NaOH in aqueous solution, respectively (Ex = 453 nm; slits: 5/10 nm). Inset (B, C): Photographs of (1) DPy-6C@SCD; (2) DPy-6C@SCD+H^+; (3) DPy-6C@SCD+OH^-. Inset (E): Photographs of (1) DPy-6C@SCD and (2) DPy-6C@SCD+OH^- under 365 nm irradiation. (F) Reversible fluorescence intensity changes of DPy-6C@SCD toward OH^- and H^+ at 593 nm in aqueous solution.

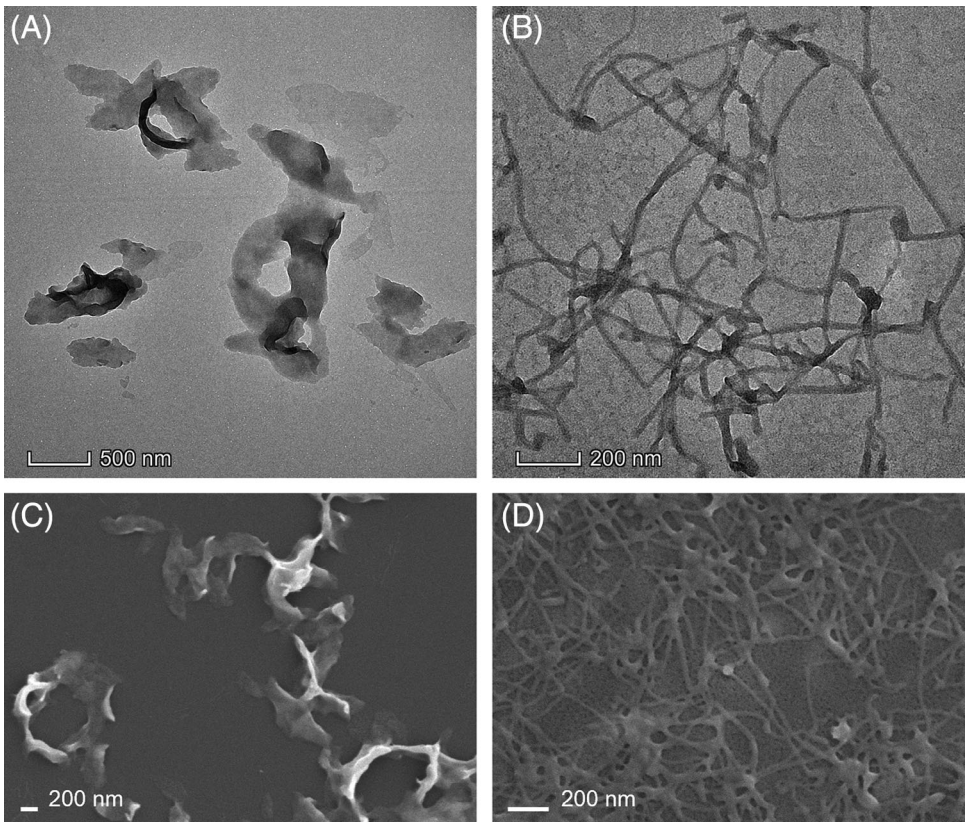

FIGURE 4 Transmission electron microscopy (TEM) and scanning electron microscopy (SEM) images of (A, C) DPy-6C@SCD+H^+; (B, C) DPy-6C@SCD+OH^-.

shown in Figure S16A, there is no significant change in DBr-6C in the presence of SCD or H^+. However, when SCD and H^+ are added at the same time, the fluorescence emission spectrum of DBr-6C@SCD shows an obvious redshift of 100 nm (Figure S16B). That is, once the tertiary amines in DBr-6C are protonated, the single-charged DBr-6C can assemble with negatively charged SCD through electrostatic interactions, thereby inducing guest molecules to assemble and leading to a redshift of fluorescence emission. Therefore, the single-charged DPy-6C becomes double-charged

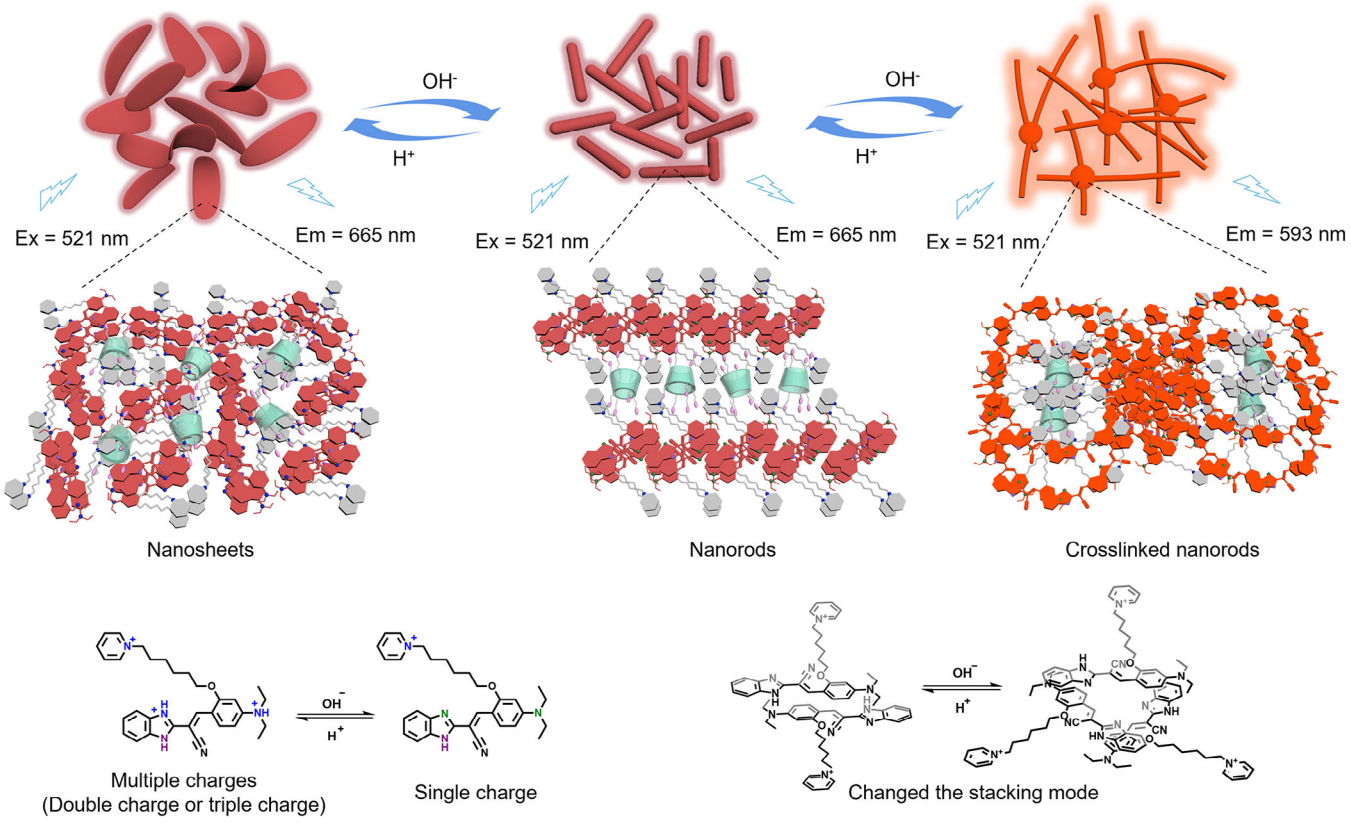

SCHEME 2 Schematic illustration of the reversible response mechanism of DPy-6C@SCD to acid and base, as well as their morphological transformation.

or triple-charged after adding the H^+ due to the secondary ammonia in both diethylamino and benzimidazole of DPy-6C can be protonated upon the addition of H^+ (Figure S17), and then further assembly with SCD to form elliptical nanosheets (Scheme 2). On the other hand, after the addition of OH^- in the DPy-6C@SCD solution, the fluorescence emission displayed a blue shift at about 72 nm and the morphology became disordered. ^{1}H-NMR of the DPy-6C@SCD and DPy-6C@SCD+OH^- (Figure S18) were performed to explore the mechanism of DPy-6C@SCD to bases. The results showed that a large number of bases can cause the protons of the aromatic group in DPy-6C to reappear, indicating that the bases can disturb the intermolecular stacking of DPy-6C, thereby resulting in the blue shift of the emission spectrum. According to the above results, it can be found that the DPy-6C@SCD displayed an obvious response to OH^-, which cannot be realized by the DPy-6C monomer. This was mainly dependent on the synergy of multiple noncovalent interactions in supramolecular assembly including electrostatic interactions, π-π stacking interactions, and hydrophobic interactions, endowing the aggregation with excellent responsiveness that cannot be achieved by monomer. Meanwhile, the fluorescence quantum yields of DPy-6C@SCD+H^+, and DPy-6C@SCD+OH^- were measured to be 0.80% and 5.33%, respectively (Figure S19). The lifetime of Py-6C@SCD+H^+, and DPy-6C@SCD+OH^- were measured to be 1.55 and 2.37 ns, respectively (Figure S20).

By using the stimulus-response performance of the DPy-6C@SCD toward OH^-, we wonder whether it can be used as a good luminescent platform for sensing volatile organic amines. Hence, some amines such as ammonium hydroxide, triethylamine, *n*-butylamine, diisopropylamine, and benzylamine were selected as the models. In liquid sensing, the diluted volatile amines solution was added to the DPy-6C@SCD solution. The fluorescence intensity of DPy-6C@SCD at 593 nm gradually enhanced with the increasing concentration of organic amines (Figure 5A and Figure S21). Meanwhile, the DPy-6C@SCD exhibited a fast response rate and can complete the detection of organic amines within 5 s (Figure S22). Based on S/N = 3,[30] the detection limit is determined to be 4.53, 15.49, 33.37, 42.47, 78.95 nM for *n*-butylamine, triethylamine, benzylamine, diisopropylamine, and ammonium hydroxide, respectively (Figure S23). On the other hand, in gas sensing, the DPy-6C@SCD solution was in an open cuvette and placed in an airtight bottle containing volatile amines at room temperature. When volatile amines are added to a closed bottle, the DPy-6C@SCD liquid surface displayed a distinct increasing orange fluorescence rapidly (Figure 5C and Videos S1–S5), accompanied by obvious enhancement of fluorescence intensity (Figure 5B). Furthermore, we used the DPy-6C@SCD to detect other organic volatile amines such as dimethylamine, trimethylamine, di-*n*-butylamine, *n*-hexylamine, and pentylamine. The result showed that DPy-6C@SCD can generate obvious fluorescence enhancement at 593 nm (Figure S24), which confirmed the universality of DPy-6C@SCD response to volatile organic amines. The results confirmed that the assembly of DPy-6C@SCD can be used as an excellent luminescent platform for fast sensing organic amines both in liquid and gas phase.

Due to the red fluorescence intensity of DPy-6C@SCD being decreased and the orange fluorescence intensity being increased in the presence of ammonium hydroxide, RGB

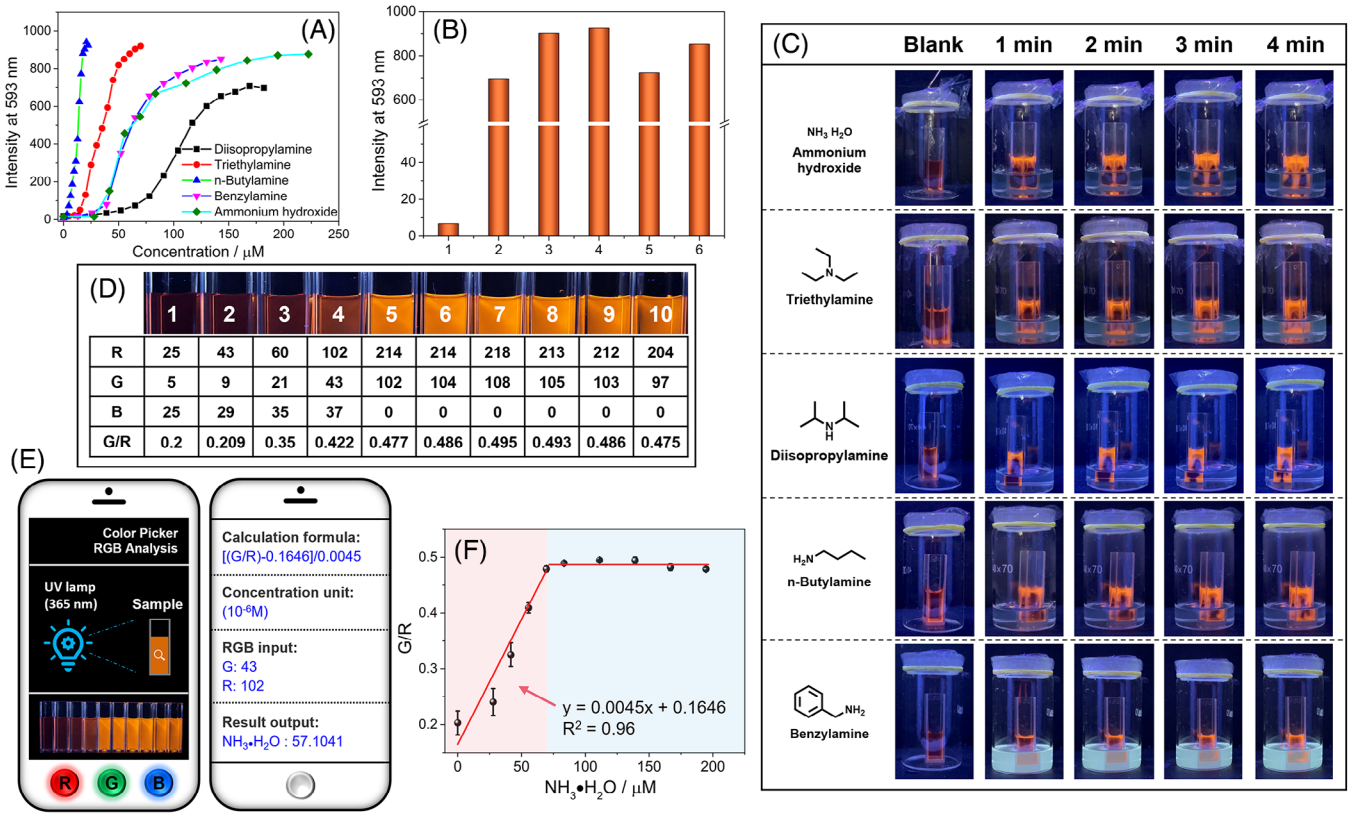

FIGURE 5 (A) The fluorescence intensity changes of DPy-6C@SCD at 593 nm with the increase of volatile amine concentration in aqueous solution (Ex = 453 nm; slits: 5/10 nm); (B) The fluorescence intensity of DPy-6C@SCD toward five volatile amines (after complete response in gas phase; (C) Representative time dependent photographs of DPy-6C@SCD after exposed to volatile amine under 365 nm irradiation; (D) Photographs of DPy-6C@SCD after adding different concentration of ammonium hydroxide (0.25%) and their R, G, B, R/G values under 365 nm irradiation; (E) Operational procedures of the RGB analysis and calculation application by using DPy-6C@SCD in smartphone platform; (F) G/R value of DPy-6C@SCD solution upon addition of ammonium hydroxide (0.25%) under 365 nm irradiation.

analysis could be used as a semi-quantitative method to intuitively determine the concentration of ammonium hydroxide. Therefore, DPy-6C@SCD was used in conjunction with a smartphone-adaptable RGB application (ColorPicker).[31] As shown in Figure 5D, the RGB analysis of different solutions was carried out by smartphone, and a good linear correlation existed between the G/R value of DPy-6C@SCD and ammonium hydroxide concentrations in the range of 0–69.5 μM (Figure 5F). Then the fitted formula was edited into the calculation application (iResult) of the smartphone, and the concentration of ammonium hydroxide can be quickly obtained by inputting the captured RGB value (Figure 5E). When the smartphone was used for RGB analysis, the concentration of ammonium hydroxide could be quickly outputted from the formula application. The results indicated that a combination of the DPy-6C@SCD sensing process with a smartphone can be used to determine ammonium hydroxide concentration without complex pretreatment and expensive instruments, providing a portable tool for visually and semi-quantitatively monitoring volatile organic amines.

3 | CONCLUSION

In summary, we constructed pH-responsive NIR aggregates based on negatively charged SCD-induced DPy-6C directed aggregation through electrostatic interactions, π-π stacking interactions, and hydrophobic interactions. In the presence of SCD, the UV-vis absorption of DPy-6C redshifted from 453 to 521 nm, accompanied by the fluorescence emission redshifted from 530 to 665 nm, and the morphology of DPy-6C changed from random nanosheets to regular nanorods. Upon addition of OH^-, DPy-6C@SCD displayed an emission blue shift of 72 nm and a 90-fold increase in intensity that cannot be achieved by the DPy-6C monomer (Table S1). The DPy-6C@SCD can serve as a good luminescent platform for rapidly sensing volatile organic amines in liquid and gas states within 5 s at the nanomolar level. Combining the identification process with a smartphone, the content of organic amines can be quickly and semi-quantitatively detected through intelligent methods. Therefore, the multicharged macrocycles induced directional aggregation strategy not only realizes the topological morphology transformation but also achieves significant emission spectrum redshift, which can be combined with a smartphone for the rapid detection of volatile organic amines, providing a convenient method for constructing supramolecular intelligent devices.

ACKNOWLEDGMENTS

We gratefully acknowledge the financial support received from the following: the National Natural Science Foundation of China (Grant Nos. 21971192 and 21807038), the Tianjin Municipal Education Commission (Grant No. 2021KJ188), and the China Postdoctoral Science Foundation (Grant No. 2021T140343).

CONFLICT OF INTEREST STATEMENT

The authors declare no conflict of interest.

ORCID

Chunju Li https://orcid.org/0000-0001-7450-4867
Yu Liu https://orcid.org/0000-0001-8723-1896

REFERENCES

1. a) C. Ortiz Mellet, J. M. Garcia Fernandez, J. M. Benito, *Chem. Soc. Rev.* **2011**, *40*, 1586. b) G. Yu, X. Zhao, J. Zhou, Z. Mao, X. Huang, Z. Wang, B. Hua, Y. Liu, F. Zhang, Z. He, O. Jacobson, C. Gao, W. Wang, C. Yu, X. Zhu, F. Huang, X. Chen, *J. Am. Chem. Soc.* **2018**, *140*, 8005.
2. a) S. Fu, X. Su, M. Li, S. Song, L. Wang, D. Wang, B. Z. Tang, *Adv. Sci.* **2020**, *7*, 2001909. b) W. Zhang, Y. M. Zhang, S. H. Li, Y. L. Cui, J. Yu, Y. Liu, *Angew. Chem. Int. Ed.* **2016**, *55*, 11452.
3. a) J. Liang, A. Hao, P. Xing, Y. Zhao, *ACS Nano* **2021**, *15*, 5322. b) Y. Li, Q. Li, X. Miao, C. Qin, D. Chu, L. Cao, *Angew. Chem. Int. Ed.* **2021**, *60*, 6744.
4. a) P. Xing, C. Yang, Y. Wang, S. Z. F. Phua, Y. Zhao, *Adv. Funct. Mater.* **2018**, *28*, 1802859. b) J. J. Li, Y. Chen, J. Yu, N. Cheng, Y. Liu, *Adv. Mater.* **2017**, *29*, 1701905. c) C. Tu, W. Wu, W. Liang, D. Zhang, W. Xu, S. Wan, W. Lu, C. Yang, *Angew. Chem. Int. Ed.* **2022**, *61*, e202203541. d) Q. Feng, S. Zhu, B. Wang, F. Yu, H. Li, M. Yu, M. Xu, L. Xie, *Adv. Funct. Mater.* **2023**, *34*, 2312622.
5. a) X. Chen, H. K. Bisoyi, X.-F. Chen, X.-M. Chen, S. Zhang, Y. Tang, G. Zhu, H. Yang, Q. Li, *Matter* **2022**, *5*, 3883. b) J. Tang, Y. Tian, Z. Lin, C. Zhang, P. Zhang, R. Zeng, S. Wu, X. Chen, J. Chen, *ACS Appl. Mater. Interfaces* **2022**, *15*, 2237.
6. a) X.-Y. Dai, M. Huo, Y. Liu, *Nat. Rev. Chem.* **2023**, *7*, 854. b) S. Garain, B. C. Garain, M. Eswaramoorthy, S. K. Pati, S. J. George, *Angew. Chem. Int. Ed.* **2021**, *60*, 19720.
7. a) J. Yi, G. Zou, J. Huang, X. Ren, Q. Tian, Q. Yu, P. Wang, Y. Yuan, W. Tang, C. Wang, L. Liang, Z. Cao, Y. Li, M. Yu, Y. Jiang, F. Zhang, X. Yang, W. Li, X. Wang, Y. Luo, X. J. Loh, G. Li, B. Hu, Z. Liu, H. Gao, X. Chen, *Nature* **2023**, *624*, 295. b) I. Roy, J. F. Stoddart, *Acc. Chem. Res.* **2021**, *54*, 1440.
8. a) Z. Wang, C. Sun, K. Yang, X. Chen, R. Wang, *Angew. Chem. Int. Ed.* **2022**, *61*, e202206763. b) J. X. Liu, K. Chen, C. Redshaw, *Chem. Soc. Rev.* **2023**, *52*, 1428. c) C. J. Yin, Z. A. Yan, R. J. Yan, C. Xu, B. B. Ding, Y. H. Ji, X. Ma, *Adv. Funct. Mater.* **2024**, 2316008. https://doi.org/10.1002/adfm.202316008. d) L. L. Tan, M. Wei, L. Shang, Y. W. Yang, *Adv. Funct. Mater.* **2020**, *31*, 2007277. e) G. Li, Y. M. Li, *Aggregate* **2022**, *3*, e161.
9. a) J. R. Wu, G. Wu, Y. W. Yang, *Acc. Chem. Res.* **2022**, *55*, 3191. b) Y. Mei, Q. W. Zhang, Q. Gu, Z. Liu, X. He, Y. Tian, *J. Am. Chem. Soc.* **2022**, *144*, 2351.
10. a) H. Duan, Y. Li, Q. Li, P. Wang, X. Liu, L. Cheng, Y. Yu, L. Cao, *Angew. Chem. Int. Ed.* **2020**, *59*, 10101. b) I. Roy, A. H. G. David, P. J. Das, D. J. Pe, J. F. Stoddart, *Chem. Soc. Rev.* **2022**, *51*, 5557. c) H. T. Feng, Y. X. Yuan, J. B. Xiong, Y. S. Zheng, B. Z. Tang, *Chem. Soc. Rev.* **2018**, *47*, 7452.
11. a) X. N. Han, Y. Han, C. F. Chen, *Chem. Soc. Rev.* **2023**, *52*, 3265. b) Z.-Y. Zhang, C. Li, *Acc. Chem. Res.* **2022**, *55*, 916.
12. a) J. S. Chen, Q. Y. Peng, X. W. Peng, H. Zhang, H. B. Zeng, *Chem. Rev.* **2022**, *122*, 14594. b) R. N. Dsouza, U. Pischel, W. M. Nau, *Chem. Rev.* **2011**, *111*, 7941.
13. a) X. Ma, J. Wang, H. Tian, *Acc. Chem. Res.* **2019**, *52*, 738. b) B. Hua, L. Shao, M. Li, H. Liang, F. Huang, *Acc. Chem. Res.* **2022**, *55*, 1025. c) R. Jiang, M. Nilam, A. Hennig, W. M. Nau, *Adv. Mater.* **2023**, *36*, 2306922.
14. a) G. Wu, F. Li, B. Tang, X. Zhang, *J. Am. Chem. Soc.* **2022**, *144*, 14962. b) H. Zhu, Q. Li, W. Zhu, F. Huang, *Acc. Mater. Res.* **2022**, *3*, 658. c) B. Schmidt, C. Barner-Kowollik, *Angew. Chem. Int. Ed.* **2017**, *56*, 8350.
15. a) H. Nie, Z. Wei, X.-L. Ni, Y. Liu, *Chem. Rev.* **2022**, *122*, 9032. b) N. Barooah, J. Mohanty, A. C. Bhasikuttan, *Chem. Commun.* **2015**, *51*, 13225.
16. a) Z. Liu, X. Dai, Y. Sun, Y. Liu, *Aggregate* **2020**, *1*, 31. b) H. Yan, X. Yin, D. Wang, T. Han, B. Z. Tang, *Adv. Sci.* **2023**, *10*, 2305149.
17. H.-J. Kim, P. C. Nandajan, J. Gierschner, S. Y. Park, *Adv. Funct. Mater.* **2018**, *28*, 1705141.
18. B. Shi, K. Jie, Y. Zhou, J. Zhou, D. Xia, F. Huang, *J. Am. Chem. Soc.* **2016**, *138*, 80.
19. a) J. J. Li, H. Y. Zhang, G. Liu, X. Dai, L. Chen, Y. Liu, *Adv. Optical Mater.* **2020**, *9*, 2001702. b) G. Singh, P. K. Singh, *Langmuir* **2019**, *35*, 14628.
20. Z. Liu, X. Sun, X. Dai, J. Li, P. Li, Y. Liu, *J. Mater. Chem. C* **2021**, *9*, 1958.
21. X. Y. Dai, Y. Y. Hu, Y. Sun, M. Huo, X. Dong, Y. Liu, *Adv. Sci.* **2022**, *9*, e2200524.
22. a) W. C. Geng, J. L. Sessler, D. S. Guo, *Chem. Soc. Rev.* **2020**, *49*, 2303. b) Z. Liu, H. Chen, L. Guo, X. Sun, Z.-Y. Zhang, J. Chen, M. Dong, C. Li, *Chin. Chem. Lett.* **2024**, *35*, 109666. c) W. Liu, S. Bobbala, C. L. Stern, J. E. Hornick, Y. Liu, A. E. Enciso, E. A. Scott, J. F. Stoddart, *J. Am. Chem. Soc.* **2020**, *142*, 3165.
23. a) Z. Liu, W. Lin, Y. Liu, *Acc. Chem. Res.* **2022**, *55*, 3417. b) W. F. Lai, A. L. Rogach, W. T. Wong, *Chem. Soc. Rev.* **2017**, *46*, 6379. c) J. Huang, J. Huang, P. Cheng, Y. Jiang, K. Pu, *Adv. Funct. Mater.* **2020**, *30*, 2003628. d) J. Wankar, N. G. Kotla, S. Gera, S. Rasala, A. Pandit, Y. A. Rochev, *Adv. Funct. Mater.* **2020**, *30*, 1909049. e) Y. J. Ooi, Y. Wen, J. Zhu, X. Song, J. Li, *Biomacromolecules* **2020**, *21*, 1136. f) X. Zhou, R. Ikura, C. Jin, K. Yamaoka, J. Park, Y. Takashima, *Aggregate* **2024**, *5*, e457. g) L. Liu, M. Zhu, J. Feng, H. Peng, Y. Shi, J. Gao, L. C. Tang, P. Song, *Aggregate* **2024**, *5*, e494. h) Z. Hu, S. Xu, H. Zhang, X. Ji, *Aggregate* **2022**, *4*, e283. i) J. Y. Ma, Y. X. Wang, Y. Huang, Y. Zhang, Y. X. Cui, D. M. Kong, *Aggregate* **2022**, *3*, e166.
24. a) L. Hu, K. Li, W. Shang, X. Zhu, M. Liu, *Angew. Chem. Int. Ed.* **2020**, *59*, 4953. b) Z. Liu, M. Tian, H. Zhang, Y. Liu, *Chem. Commun.* **2023**, *59*, 896. c) Z. Liu, H. Chen, X. Sun, J. Lu, J. Wu, Y. Shang, Z. Y. Zhang, C. Li, *Asian J. Org. Chem.* **2024**, *13*, e202300663. d) Q. Wang, Q. Zhang, Q. W. Zhang, X. Li, C. X. Zhao, T. Y. Xu, D. H. Qu, H. Tian, *Nat. Commun.* **2020**, *11*, 158.
25. a) Q. W. Zhang, D. Li, X. Li, P. B. White, J. Mecinovic, X. Ma, H. Agren, R. J. M. Nolte, H. Tian, *J. Am. Chem. Soc.* **2016**, *138*, 13541. b) M. Tang, Y. H. Liu, H. Liu, Q. Mao, Q. Yu, H. Kitagishi, Y. M. Zhang, L. Xiao, Y. Liu, *J. Med. Chem.* **2022**, *65*, 13473.
26. a) Z. Liu, Y. Liu, *Chem. Soc. Rev.* **2022**, *51*, 4786. b) M. D. Tian, Z. Wang, X. Yuan, H. Zhang, Z. X. Liu, Y. Liu, *Adv. Funct. Mater.* **2023**, *33*, 2300779.
27. Y. Y. Hu, X. Y. Dai, X. Dong, M. Huo, Y. Liu, *Angew. Chem. Int. Ed.* **2022**, *61*, e202213097.
28. a) Y. M. Zhang, Y. H. Liu, Y. Liu, *Adv. Mater.* **2020**, *32*, 1806158. b) A. Blanco-Gómez, P. Cortón, L. Barravecchia, I. Neira, E. Pazos, C. Peinador, M. D. García, *Chem. Soc. Rev.* **2020**, *49*, 3834.
29. a) G. Han, D. Kim, Y. Park, J. Bouffard, Y. Kim, *Angew. Chem. Int. Ed.* **2015**, *54*, 3912. b) T. I. Kim, H. Jin, J. Bae, Y. Kim, *Anal. Chem.* **2017**, *89*, 10565. c) Y. Li, L. Ning, F. Yuan, T. Zhang, J. Zhang, Z. Xu, X. F. Yang, *Anal. Chem.* **2020**, *92*, 5733. d) T. I. Kim, Y. Kim, *Chem. Commun.* **2016**, *52*, 10648. e) S. Ma, S. Du, G. Pan, S. Dai, B. Xu, W. Tian, *Aggregate* **2021**, *2*, e96.
30. a) H. Zhu, J. Fan, J. Wang, H. Mu, X. Peng, *J. Am. Chem. Soc.* **2014**, *136*, 12820. b) Z. Liu, X. Dai, Q. Xu, X. Sun, Y. Liu, *Chin. J. Chem.* **2022**, *40*, 493.
31. a) J. Zhang, Y. Yang, L. Zeng, J. Wang, *Food Chem.* **2024**, *436*, 137769. b) H. Ye, S. Koo, Z. Beitong, Y. Ke, R. Sheng, T. Duan, L. Zeng, J. S. Kim, *Anal. Chem.* **2022**, *94*, 15423. c) Pratibha, A. Kapoor, J. K. Rajput, A. Kumar, *Anal. Chem.* **2022**, *94*, 17685. d) Z. Xu, C. Zeng, Y. Zhao, M. Zhou, T. Lv, C. Song, T. Qin, L. Wang, B. Liu, X. Peng, *Food Chem.* **2023**, *410*, 135381.

SUPPORTING INFORMATION

Additional supporting information can be found online in the Supporting Information section at the end of this article.

How to cite this article: Z. Liu, H. Chen, M. Tian, X. Sun, Y.-X. Li, J. Wu, R. Wang, B. Li, C. Li, Y. Liu, *Aggregate* **2024**, e627. https://doi.org/10.1002/agt2.627